Inorganic Chemistry

Article

pubs.acs.org/IC

Monopicolinate-dipicolyl Derivative of Triazacyclononane for Stable Complexation of Cu^{2+} and $^{64}Cu^{2+}$

Melissa Roger,[†] Luís M. P. Lima,[‡] Mathieu Frindel,[§,†] Carlos Platas-Iglesias,*[,∥] Jean-François Gestin,[§] Rita Delgado,*[,‡] Véronique Patinec,[†] and Raphaël Tripier*[,†]

[†]Université de Bretagne Occidentale, UMR-CNRS 6521, UFR des Sciences et Techniques, 6 avenue Victor le Gorgeu, C.S. 93837, 29238 Brest Cedex 3, France

[‡]Instituto de Tecnologia Química e Biológica, Universidade Nova de Lisboa, Av. da República, 2780-157 Oeiras, Portugal

[§]Institut de Recherche Thérapeutique IRT, UN Unité INSERM 892-CNRS 6299, Centre de Recherche en Cancérologie Nantes-Angers, 8 quai Moncousu, BP70721 44007 Nantes Cedex, France

[∥]Departamento de Química Fundamental, Universidade da Coruña, Campus da Zapateira, Rúa da Fraga 10, 15008 A Coruña, Spain

Supporting Information

ABSTRACT: The synthesis and characterization of H**no1p-a2py**, a new tacn-based ligand, is reported. The complexation process with Cu^{2+} was proved to be very fast even in acidic medium. Potentiometric titrations allowed us to establish that H**no1pa2py** exhibits an overall low basicity as well as a high selectivity for Cu^{2+} over Zn^{2+} cations. The copper(II) complex was synthesized and characterized using UV−vis and EPR spectroscopies and density functional theory (DFT) calculations. The studies clearly showed that the $[Cu(\mathbf{no1pa2py})]^+$ complex is present in solution as a mixture of two isomers in which the ligand is coordinated to the metal center using a N_5O donor set with the metal center in a distorted octahedral geometry. The very high kinetic inertness of the $[Cu(\mathbf{no1pa2py})]^+$ complex was demonstrated by using acid-assisted dissociation assays as well as cyclic voltammetry. Preliminary investigations of ^{64}Cu complexation were performed to validate the potential use of such chelating agent for further application in nuclear medicine. The X-ray crystal structures of copper(II) complexes of **L1**, the ester derivative of H**no1pa2py**, have been determined.

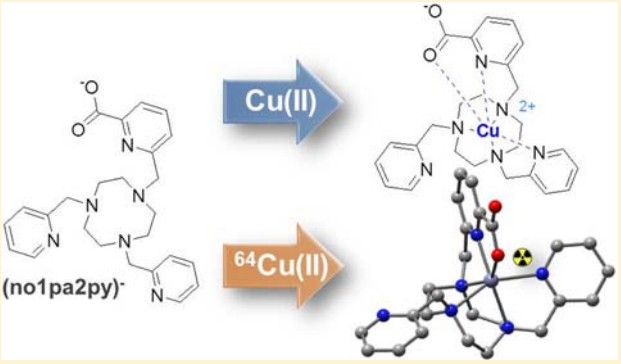

INTRODUCTION

In the past years a great deal of research has been conducted to develop radiopharmaceuticals for application in imaging and therapy of tumors. Among the radioisotopes that can be produced nowadays in high yield by a cyclotron is ^{64}Cu ($t_{1/2}$ 12.7 h), which presents an interesting biologically viable half-life decay and a low β^+ energy suitable for positron emission tomography (PET).[1] Such characteristics have prompted the design of a variety of ^{64}Cu-based bifunctional chelating agents (BCA) for imaging applications.[2] A suitable BCA should provide a fast complexation of ^{64}Cu as well as a high thermodynamic stability and kinetic inertness to avoid possible transchelation and transmetalation in biological media.[3] Moreover, bioreduction of Cu^{2+} to Cu^+ constitutes an additional possible pathway for the demetalation of the chelate that should be considered in the design of an ideal BCA.[4]

The family of cyclic polyamines provides a wide range of platforms useful for the design of progressively improved BCAs.[5] The easily accessible and well-known H_4dota and H_4teta chelators proved their ability to form complexes of Cu^{2+} with very high thermodynamic stability ($\log K_{CuL} > 21$)[6] but presented limited kinetic inertness to avoid demetalation,[7] which leads to the accumulation of ^{64}Cu in organs.[8] In order to overcome the lack of kinetic inertness of the tetraazamacrocyclic complexes, cage-like polyaza chelators such as bicyclic hexaamines,[9] dicarboxylic acid cross-bridged cyclen (H_2cb-do2a),[10] cyclam (H_2cb-te2a),[11] and other derivatives[12] were subsequently developed (Chart 1). However, in spite of the inertness of these complexes to the dissociation they exhibit slow formation rates, which is a serious drawback for the aimed biological applications. Introduction of picolinate arms on the chelate framework has also been explored as a strategy for improving thermodynamic stability and kinetic inertness. Recently, the copper(II) complex of the noncyclic dipicolinate diamine H_2dedpa (also called H_2bcpe) showed too low kinetic and thermodynamic stability for in vivo applications.[13,14] Nevertheless, the cyclic polyamines cyclen and cyclam bearing one picolinate arm (Hdompa and Htempa, Chart 1)[15] were found to provide very attractive properties to their corresponding copper(II) complexes, namely high thermodynamic

Received: January 23, 2013
Published: April 12, 2013

   dx.doi.org/10.1021/ic400174r | *Inorg. Chem.* 2013, 52, 5246−5259

Chart 1. Structure of the Ligands Discussed in This Work

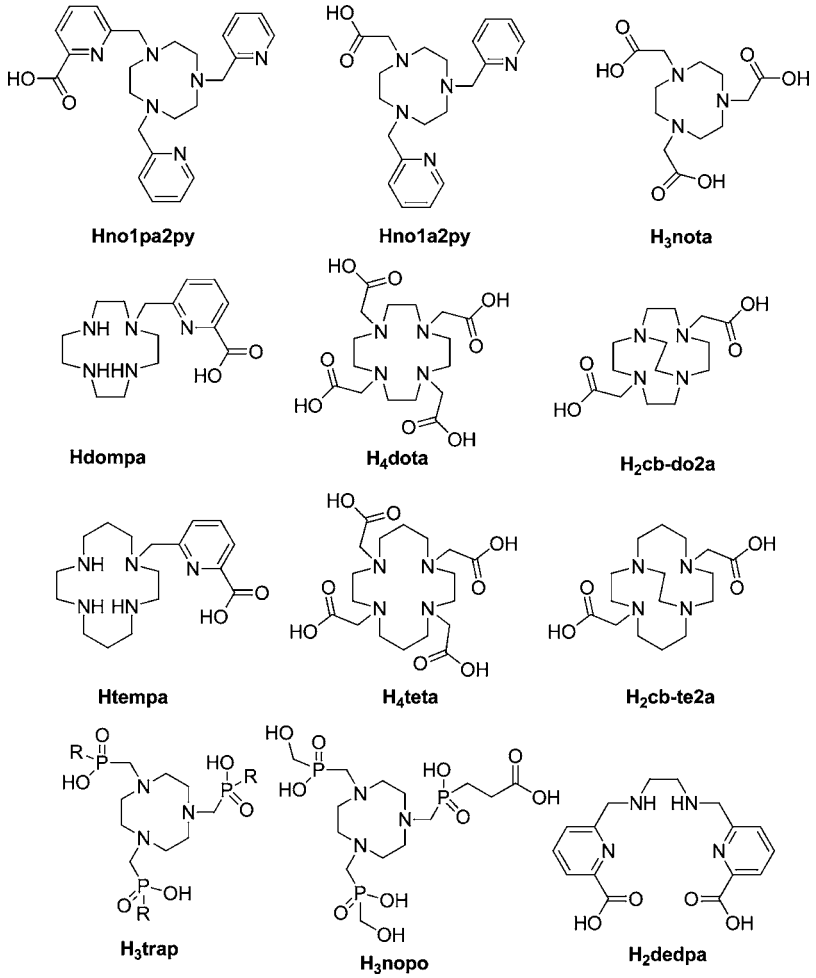

stability, kinetic inertness, fast complexation rates, and electrochemical stability upon copper(II) reduction.

Trisubstituted triazamacrocyclic derivatives based on the triazacyclononane (tacn) platform have also been applied in copper(II) complexation studies, in particular those with acetic acid (H_3nota)[16] or methylenephosphinic (H_3trap, H_3nopo)[17,18] arms. It has been reported that a ^{64}Cu- nota peptide conjugate showed better *in vivo* stability than the ^{64}Cu-dota homologue,[19] offering an interesting way to explore development of new BCAs. Recent studies with H_3trap and H_3nopo showed neighboring properties to those of H_3nota for ^{64}Cu labeling.[20] Another way to stabilize the complex of Cu^{2+} is by addition of nitrogen donors, such as picolyl groups, as coordinating units. A N_5O coordinating triazacyclononane derivative (Hno1a2py), bearing two picolyl and one acetic acid arms, showed capacity to form a stable ^{64}Cu complex with no evidence of transchelation or demetalation.[21] The bombesin bioconjugate of its ^{64}Cu complex also exhibited low activity accumulation in the liver tissue and an extensive renal clearance.[22] The replacement of the carboxylate pendant arm by a picolinate group on the previous N_5O triazamacrocycle should enhance the stability of its copper(II) complex. Indeed, azamacrocycles with picolinate pendant arms have demonstrated their ability to form stable complexes with different transition metal or lanthanide cations.[13−15,23] The new chelate should offer a N_6 or N_5O coordination mode to the metal center, thereby providing the opportunity to prepare BCAs via functionalization of either a nitrogen atom of the tacn unit or the carboxylic acid group of the picolinate fragment.

Herein we report the synthesis and characterization of the tacn-based ligand H**no1pa2py** (Chart 1). The acid−base properties of this ligand and the stability constants of its complexes with Cu^{2+} and Zn^{2+} were determined. The complex of Cu^{2+} was synthesized and characterized using cyclic voltammetry, UV−vis and electron paramagnetic resonance (EPR) spectroscopies, and density functional theory (DFT) calculations. The kinetic stability of this complex was also studied in acidic conditions, while preliminary ^{64}Cu complexation experiments were performed to validate the potential use of such chelator for further applications in nuclear medicine. Finally, structures of copper(II) complexes of the methyl ester derivative of H**no1pa2py** have been determined by X-ray diffraction on single crystals obtained from solutions of the complex at different pH values.

RESULTS AND DISCUSSION

Ligand Synthesis. The synthesis of the tacn derivative 1,4-bis(pyridinemethyl)triazacyclononane (**5**) was achieved in five steps involving the stepwise introduction of two picolyl groups in the tacn unit (Scheme 1). The synthesis of **5** was already described by two different groups with only slight modifications.[22,24] In the present work a very similar approach to that reported by Spiccia et al.[22] was used, consisting of the formation of an orthoamide intermediate **1** by reaction of tacn

dx.doi.org/10.1021/ic400174r | Inorg. Chem. 2013, 52, 5246−5259

Scheme 1. Synthesis of Hno1pa2py

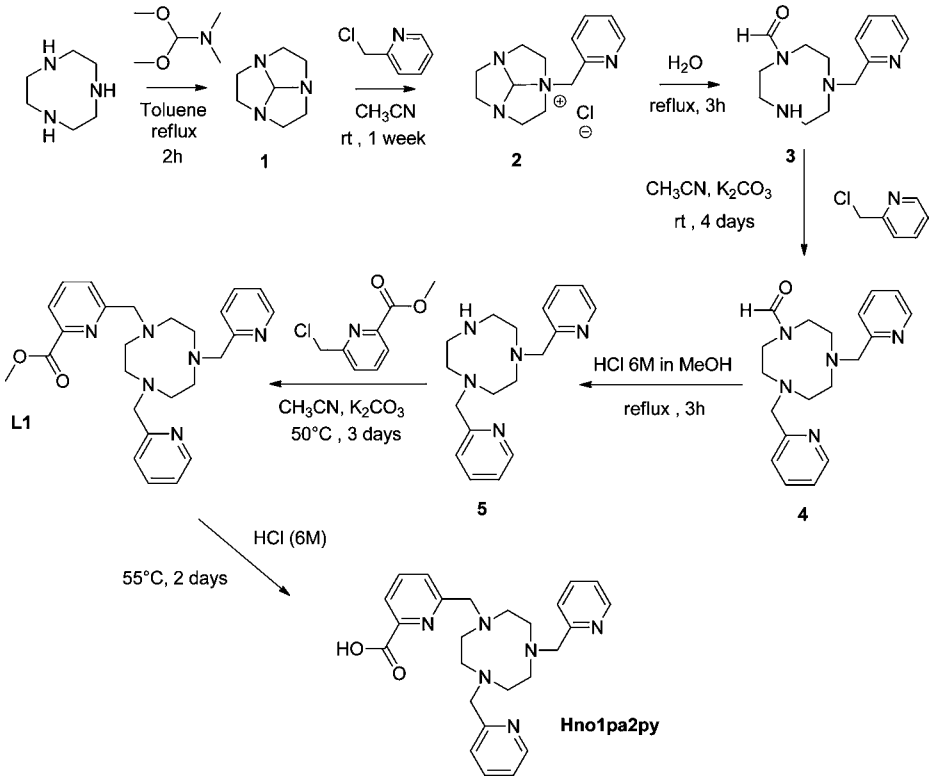

with *N*-dimethoxymethyl-*N*,*N*-dimethylamine. Addition of 2-(chloromethyl)pyridine led to the corresponding ammonium salt **2**, whose neutral hydrolysis resulted in an intermediate with only one secondary amine function available for *N*-alkylation (**3**, Scheme 1). This intermediate was allowed to react with a second equivalent of 2-(chloromethyl)pyridine to give **4**, followed by hydrolysis with 6 M HCl in methanol to give compound **5** in 60% overall yield as calculated from tacn. This yield represents a significant improvement when compared with that reported by Spiccia et al. (46%), presumably because the different intermediates shown in Scheme 1 were not isolated and were used in the next step without further purification. However, the strategy and yield obtained in this work are very similar to those reported by Hasserodt et al. (59%),[24] the only difference being that **5** was obtained after basic, rather than acid, hydrolysis of the formylated precursor. Reaction of compound **5** with 6-chloromethylpyridine-2-carboxylic acid methyl ester[25] gave compound **L1** with excellent yield (93%). Finally, the hydrolysis of **L1** with 6 M HCl led to H**no1pa2py** as a hydrochloride salt in 94% yield.

Complexes of L1 with Cu^{2+} and Their X-ray Crystal Structures. Attempts to obtain single crystals of the complex of Cu^{2+} with H**no1pa2py** suitable for X-ray diffraction analysis were unsuccessful. However, single crystals of two complexes of **L1**, which contains a methyl ester group instead of a carboxylate function, were obtained. The complexes of **L1** could actually be considered as a realistic model of any putative conjugates where the carboxylate functional group is used for conjugation with peptides/proteins. These crystals were isolated after reaction of H**no1pa2py** with $Cu(ClO_4)_2{\cdot}6H_2O$ in aqueous solutions at pH values 1.5 and 4.5, respectively, followed by addition of methanol. A view of the structure of the complex $[Cu\mathbf{L1}](ClO_4)_2{\cdot}H_2O$ (**6**) obtained at pH 4.5 is shown in Figure 1, while bond distances and angles of the metal

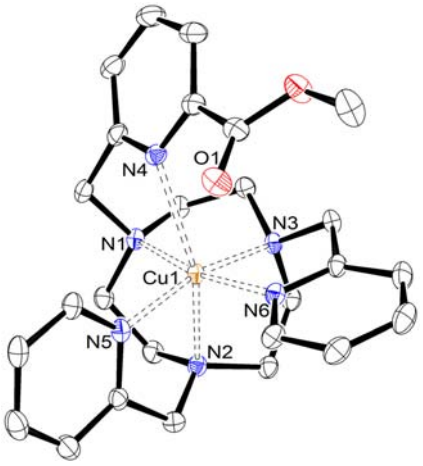

Figure 1. View of the crystal structure of $[Cu\mathbf{L1}](ClO_4)_2{\cdot}H_2O$ (**6**). Perchlorate anions, water molecules and hydrogen atoms are omitted for clarity. The ORTEP plot is are at the 30% probability level.

coordination environment are collected in Table 1. The structure of complex $[Cu(H\mathbf{L1})Cl](ClO_4)_2{\cdot}H_2O$ (**7**) obtained at pH 1.5, together with bond distances, angles, and description, is given in the Supporting Information (Figure S1 and Tables S1, S2).

Crystals of compound $[Cu\mathbf{L1}](ClO_4)_2{\cdot}H_2O$ (**6**) are composed of the cationic entity $[Cu\mathbf{L1}]^{2+}$, two perchlorate anions, and a water molecule involved in hydrogen-bonding interactions with the perchlorate anions. The metallic atom is hexacoordinated, and the complex structure exhibits a distorted octahedral geometry with the copper center coordinated to three nitrogen atoms of the triazamacrocycle, two nitrogen atoms from the picolyl substituents and the nitrogen atom of

dx.doi.org/10.1021/ic400174r | *Inorg. Chem.* 2013, 52, 5246−5259

Table 1. Selected Bond Lengths (Å) and Angles (deg) of the Metal Coordination Environments in $[CuL1](ClO_4)_2 \cdot H_2O$ (6)[a]

Cu(1)−N(1)	2.084(3)	N(5)−Cu(1)−N(3)	164.87(12)
Cu(1)−N(2)	2.235(3)	N(6)−Cu(1)−N(1)	166.69(12)
Cu(1)−N(3)	2.040(3)	N(5)−Cu(1)−N(1)	97.03(12)
Cu(1)−N(4)	2.504	N(3)−Cu(1)−N(1)	85.02(12)
Cu(1)−N(5)	2.009(3)	N(6)−Cu(1)−N(2)	101.56(12)
Cu(1)−N(6)	2.008(3)	N(5)−Cu(1)−N(2)	80.67(12)
N(6)−Cu(1)−N(5)	96.17(12)	N(3)−Cu(1)−N(2)	84.78(12)
N(6)−Cu(1)−N(3)	82.67(12)	N(1)−Cu(1)−N(2)	82.29(12)

[a]See Figure 1 for labeling.

the picolinate ester group. The oxygen atom of the picolinate ester group remains uncoordinated. The coordination polyhedron around the metal ion can be considered to be composed of two nearly parallel planes: the nitrogen atoms of the tacn unit (N1, N2, and N3) define the lower plane, while the nitrogen atoms of the pyridyl units (N4, N5, and N6) delineate the upper plane. The mean twist angle of the upper and lower tripods amounts to 43.1°, which is evidence of an important degree of distortion of the coordination polyhedron from an octahedron (ideal value 60°) to a trigonal prism (ideal value 0°). As a result of this distortion, several bond angles (N1−Cu1−N2, 82.29°; N3−Cu1−N4, 97.91°; N2−Cu1−N4, 157.46°) differ significantly from those expected for an ideal octahedral coordination. A smaller twist angle (26.6°) has been reported for the $[Cu(nota)]^-$ complex,[26] which is probably related to the more important steric requirements of the pendant arms of **L1** compared to those of H_3nota. The Cu−N bond lengths are in the range 2.003−2.084 Å for N1, N3, N5, and N6, and considerably longer for N2 (2.235 Å) and N4 (2.504 Å). A similar coordination environment has been reported for $[Cu(tacn3py)]^{2+}$.[27]

The conformation adopted by the ligand in the $[CuL1]^{2+}$ complex implies the occurrence of two helicities (one belonging to the tacn moiety and the other associated with the layout of the three pendant arms).[28,29] Inspection of the crystal structure data reveals that two $\Delta(\lambda\lambda\lambda)$ and $\Lambda(\delta\delta\delta)$ enantiomers cocrystallize in equal amounts (racemate). Identical conformations were observed in the X-ray structure of $[Cu(nota)]^-$[30] and related complexes of Cu^{2+}.[31]

Acid−Base Behavior of Hno1pa2py. The acid−base reactions of the compound H**no1pa2py** were studied in aqueous solution and the protonation constants determined by potentiometric titrations. The ligand has seven basic centers (three tertiary amines of the tacn unit, three nitrogen atoms of the pyridyl groups, and an oxygen atom of the carboxylate), from which only four accurate constants could be determined by potentiometric measurements (Table 2). The compound exhibits low overall basicity because it has only one high protonation constant, which corresponds to the protonation of one amine in the macrocycle. The second one corresponds to the protonation of another amine of the cycle, presenting a low value for an amine protonation (log K = 5.25) due to the strong electrostatic repulsions of charged amines placed at short distance because of the small cavity size of the macrocycle. The other two constants determined correspond to the protonation of nitrogen atoms of the arms. Values of the same order were found for other 9-membered macrocycles such as tacn[32] and H_3nota^{3-}.[16a,33] In the speciation diagram, shown in Figure 2, it can be observed that the only species present in solution at physiological pH is the monoprotonated one.

Table 2. Overall (β_i^H) and Stepwise (K_i^H) Protonation Constants (in log Units) of Hno1pa2py, tacn, and H_3nota at 298.2 ± 0.1 K in 0.10 M KNO_3

equilibrium reaction	L = **no1pa2py**$^{-a}$	L = tacn[b]	L = nota^{3-}[c,d]
	log β_i^H		
$L + H^+ \rightleftarrows HL$	10.61(2)	10.42	11.41;[c] 11.73[d]
$L + 2H^+ \rightleftarrows H_2L$	15.86(5)	17.30	17.15;[c] 17.47[d]
$L + 3H^+ \rightleftarrows H_3L$	19.55(5)	<18.3	20.31;[c] 20.63[d]
$L + 4H^+ \rightleftarrows H_4L$	21.16(9)		22.02;[c] 22.59[d]
	log K_i^H		
$L + H^+ \rightleftarrows HL$	10.61	10.42	11.41;[c] 11.73[d]
$HL + H^+ \rightleftarrows H_2L$	5.25	6.88	5.74[c,d]
$H_2L + H^+ \rightleftarrows H_3L$	3.69	<1	3.16[c,d]
$H_3L + H^+ \rightleftarrows H_4L$	1.61		1.71;[c] 1.96[d]

[a]This work. Values in parentheses are standard deviations in the last significant figures. [b]I = 0.1 M KNO_3.[33] [c]I = 0.1 M $NaNO_3$.[34] [d]I = 0.1 M $NaNO_3$.[16a]

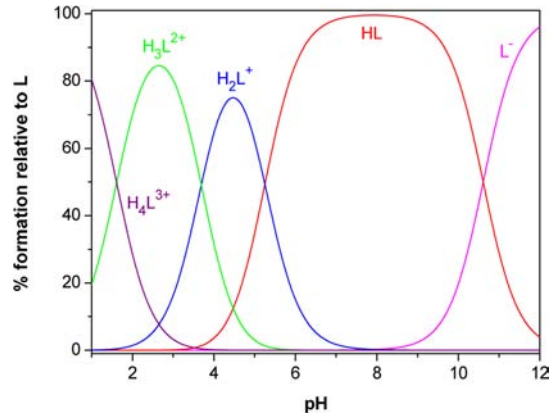

Figure 2. Speciation diagram of H**no1pa2py** in aqueous solution for $C_{Hno1pa2py} = 10^{-3}$ M.

Studies of the Copper(II) and Zinc(II) Complexes with Hno1pa2py. *Determination of Stability Constants.* The stability constants of the complexes formed by H**no1pa2py** with Cu^{2+} and Zn^{2+} metal ions were determined using potentiometric titrations at T = 298.2 K and in 0.10 M KNO_3 aqueous solutions (Table 3). The stability of the complex formed with Zn^{2+} was investigated taking into account that this cation exists in biological media in significant concentrations and generally forms thermodynamically stable complexes with ligands containing nitrogen and oxygen donor atoms. The formation of complexes with both Cu^{2+} and Zn^{2+} was found to be fast, with almost no free metal ion present in

dx.doi.org/10.1021/ic400174r | Inorg. Chem. 2013, 52, 5246−5259

Table 3. Overall ($\beta_{M_mH_hL_l}$) and stepwise ($K_{M_mH_hL_l}$) stability constants (in log units) of complexes of Hno1pa2py, tacn and H_3nota with Cu^{2+} and Zn^{2+} cations, at 298.2 ± 0.1 K in I = 0.10 ± 0.01 M KNO_3

equilibrium reaction[a]	L = **no1pa2py**[b]	L = tacn[d,e]	L = nota[3-e,f]
log $\beta_{M_mH_hL_l}$			
$Cu^{2+} + L + H^+ \rightleftarrows CuHL$	23.67(3)		24.37[f]
$Cu^{2+} + L \rightleftarrows CuL$	20.96(5)[c]	15.52;[d] 15.4[e]	21.63[f]
$Cu^{2+} + L \rightleftarrows CuLOH + H^+$	9.65(4)	9.97[d]	
$Cu^{2+} + 2L \rightleftarrows CuL_2$		27.4[e]	
$Zn^{2+} + L + H^+ \rightleftarrows ZnHL$	19.0(1)		
$Zn^{2+} + L \rightleftarrows ZnL$	16.49(6)	11.62;[d] 11.3[e]	18.3[e]
$Zn^{2+} + L \rightleftarrows ZnLOH + H^+$	5.30(7)		
$Zn^{2+} + 2L \rightleftarrows ZnL_2$		20.5[e]	
log $K_{M_mH_hL_l}$			
$CuL + H^+ \rightleftarrows CuHL$	2.71		2.74[f]
$Cu^{2+} + L \rightleftarrows CuL$	20.96[c]	15.52;[d] 15.4[e]	21.63[f]
$CuL + L \rightleftarrows CuL_2$		12.01[e]	
$CuLOH + H^+ \rightleftarrows CuL$	11.31	5.55[d]	
$ZnL + H^+ \rightleftarrows ZnHL$	2.51		
$Zn^{2+} + H^+ \rightleftarrows ZnHL$	16.49	11.62;[d] 11.3[e]	18.3[e]
$ZnLOH + H^+ \rightleftarrows ZnL$	11.19		
$Zn^{2+} + 2L \rightleftarrows ZnL_2$		9.2	

[a]The charges of L and complexes are omitted to comprise the three different ligands considered. [b]Values in parentheses are standard deviations in the last significant figures. [c]The value of $K_{Cuno1pa2py}$ was determined by competition with H_4edta by titration in H**no1pa2py**/Cu^{2+}/H_4edta 1/0.9/1.2. [d]I = 0.1 M $NaNO_3$.[33] [e]I = 0.1 M.[35] [f]I = 0.1 M $NaNO_3$.[16a]

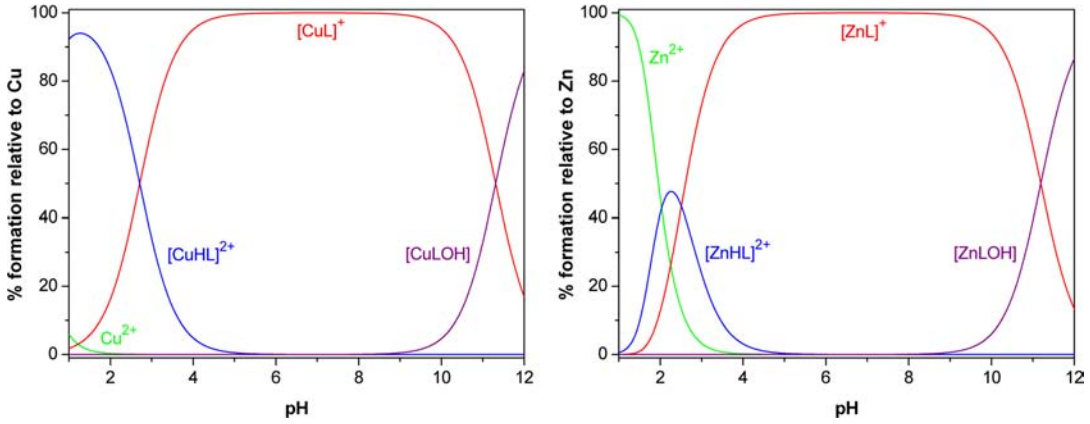

Figure 3. Speciation diagrams of Cu^{2+} (left) and Zn^{2+} (right) in presence of H**no1pa2py**. $[Cu^{2+}]_{tot}$ = $[$H**no1pa2py**$]_{tot}$ = 10^{-3} M and $[Zn^{2+}]_{tot}$ = $[$H**no1pa2py**$]_{tot}$ = 10^{-3} M.

solution above pH 2 for Cu^{2+} and above pH 4 for Zn^{2+} (see the speciation diagrams shown in Figure 3). For the complexes of Cu^{2+} it was not possible to determine the stability constants by direct potentiometry due to the almost complete formation of the complex at low pH, and therefore, they were obtained by competition titrations using H_4edta (ethylenediaminetetracetic acid) for which reliable constant values are available for our experimental conditions.[34]

Besides the [M(**no1pa2py**)]$^+$ species, the potentiometric data also evidence formation of monoprotonated complexes at very low pH, while at high pH (>10) deprotonation of one water molecule leads to the additional formation of hydroxo complexes.

The stability constants of the complexes of H**no1pa2py** with the studied metal ions are very high, being >10^5 larger than those of the parent amine tacn,[33,35] although slightly lower than those of H_3nota.[6,16a] On the other hand, H**no1pa2py** exhibits a higher selectivity for Cu^{2+} over Zn^{2+} than H_3nota. However, comparison of the complexation ability of ligands with different basicity is not correct if the competition of the ligands for the proton is not taken into account. Thus, the pM values calculated for the complexes of Cu^{2+} and Zn^{2+} with H**no1pa2py** and related ligands at physiological pH are shown in Table 4. The pCu value for the complex of H**no1pa2py** is slightly larger than that for the H_3nota analogue,

dx.doi.org/10.1021/ic400174r | Inorg. Chem. 2013, 52, 5246−5259

and furthermore, the former ligand is more selective for Cu^{2+} in presence of Zn^{2+}.

Table 4. Calculated pM[a] Values for the Complexes of Hno1pa2py, tacn, and H_3nota

metal ion	Hno1pa2py	tacn	H_3nota
Cu^{2+}	17.75	14.24	17.61
Zn^{2+}	13.28	8.17	14.28

[a]Values calculated at pH = 7.4 for 100% excess of ligand with $[M^{2+}]_{tot} = 1 \times 10^{-3}$ M, based on the constants of Tables 2 and 3.

DFT Calculations. Attempts to obtain single crystals of the complexes of H**no1pa2py** with Cu^{2+} and Zn^{2+} suitable for X-ray diffraction studies were unsuccessful. To obtain information on the structure in solution of these complexes, the $[Zn(\mathbf{no1pa2py})]^+$ and $[Cu(\mathbf{no1pa2py})]^+$ systems were characterized by means of density functional theory (DFT) calculations with the TPSSh model. In these calculations solvent effects (water) were taken into account by using a polarizable continuum model (PCM). Test calculations performed on the $[Cu\mathbf{L1}]^{2+}$ system provide a minimum energy conformation that resembles the corresponding X-ray crystal structure. The calculated bond distances between the metal ion and the coordinating donor atoms of the ligand are in very good agreement with the ones found in the crystal structure (see Supporting Information, Table S3) with an average unsigned deviation of only 2.4%. The largest deviation corresponds to the Cu−N1 distance, which amounts to 2.167 and 2.084 Å in the calculated and experimental structures, respectively. Thus, it was concluded that our DFT calculations provide a good structural agreement with the reference X-ray data.

Our DFT calculations provided two minimum energy conformations for the $[Zn(\mathbf{no1pa2py})]^+$ and $[Cu(\mathbf{no1pa2py})]^+$ systems with relative energies below 1.0 kcal mol^{-1}. These minimum energy structures differ by the overall folding of the ligand around the metal ion, which results in $\Lambda(\delta\delta\delta)$ or $\Delta(\delta\delta\delta)$ conformations (Figure 4). In both

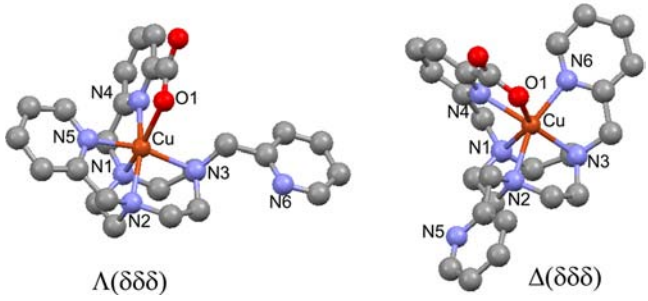

Figure 4. Geometries of the $[Cu(\mathbf{no1pa2py})]^+$ system optimized in aqueous solution at the TPSSh/SVP level.

structures the metal ion is six-coordinated in a heavily distorted octahedral environment. In the $\Lambda(\delta\delta\delta)$ conformation the nitrogen atom of one of the picolyl pendant arms (N6) remains uncoordinated, while for the $\Delta(\delta\delta\delta)$ form N5 does not coordinate to Cu^{2+} or Zn^{2+}. According to our calculations the $\Delta(\delta\delta\delta)$ form is more stable than the $\Lambda(\delta\delta\delta)$ one by 0.22 kcal mol^{-1} (Cu) and 0.98 kcal mol^{-1} (Zn).

In the $\Lambda(\delta\delta\delta)$ conformation one of the equatorial planes of the octahedron is defined by two nitrogen atoms of the tacn unit (N2 and N1) and the donor atoms of the picolinate arm N4 and O1 (mean deviation form planarity 0.12 and 0.10 Å for the Zn and Cu complexes, respectively). The *trans* angle N5−M−N3 (157.8 and 165.2° for the Zn and Cu complexes, respectively; Table 5) deviates considerably from the expected value for a regular octahedron (180°). Three of the *cis* angles of this equatorial plane are considerably smaller than the ideal value of 90°, while the fourth *cis* angle of the equatorial plane is considerably larger [N2−M−O1 = 128.4° (Zn) and 123.8° (Cu)]. All these data point to important distortions of the metal coordination environments for both complexes (Table 5).

The octahedral coordination environment is even more distorted in the case of the $\Delta(\delta\delta\delta)$ form, particularly in the case of the Zn^{2+} complex. One of the equatorial planes of the octahedron is delineated by N1, N3, N4, and O1 [mean deviation from planarity 0.26 (Zn) and 0.24 Å (Cu)]. The *trans* angles N2−M−N6 [150.2 and 158.4° for the Zn and Cu complexes, respectively], as well as the *cis* angles N3−M−O1 [133.5° (Zn) and 137.3° (Cu)] point to heavily distorted octahedral environments.

In the case of $[Cu(\mathbf{no1pa2py})]^+$, EPR measurements point to the presence of two complex species in solution (see below), which presumably correspond to the $\Lambda(\delta\delta\delta)$ and $\Delta(\delta\delta\delta)$ isomers. For the Zn^{2+} analogue the presence of two species in solution is also compatible with the experimentally observed ^{13}C and ^1H NMR spectra recorded in D_2O in the temperature range 5−45 °C, which show broad signals that point to the presence of relatively fast intramolecular conformational exchange processes (Supporting Information, Figures S3 and S4). Most likely this exchange process corresponds to the $\Lambda(\delta\delta\delta) \leftrightarrow \Delta(\delta\delta\delta)$ interconversion, which involves the rotation of the three pendant arms of the ligand. Additional ^{13}C and ^1H NMR spectra were recorded in d_7-DMF solution at different temperatures ranging from 45 °C to −40 °C (Figure S4, Supporting Information). However, the spectra recorded at −40 °C showed broad signals, indicating that the slow-exchange region for the dynamic process responsible for line-broadening is not achieved even at −40 °C. The ^1H NMR spectrum recorded at this temperature showed two set of signals in the range 7.5−9.0 ppm with clearly different intensities, which is in line with the presence of two complex species in solution.

Electronic, Infrared, and X-band EPR Spectra of the Copper(II) Complex of Hno1pa2py. The electronic spectra of the complex of Cu^{2+} with H**no1pa2py** recorded at pH 6.85 and 9.40 exhibit a broad band in the visible region centered at 652 nm (ε = 117 M^{-1} cm^{-1}) due to the copper(II) d−d transitions. Upon lowering the pH to 1.95, the maximum has a slight blue shift to 641 nm with the ε value unchanged.

The infrared spectrum of the prepared $[Cu(\mathbf{no1pa2py})](ClO_4)$ complex exhibits the characteristic carbonyl frequencies for a coordinated carboxylate group of the picolinate moiety. The strong bands around 1635−1598 cm^{-1} and at 1381 cm^{-1} were, respectively, assigned to antisymmetric and symmetric stretching vibrations of the carboxylate group, thus pointing to the involvement of the carboxylate in the coordination of the metal.

The X-band EPR spectra of frozen aqueous samples of the complex at 90 K showed a pH dependence, indicating the presence of two paramagnetic species in equilibrium throughout the entire pH range. At pH 6.85 (Figure 5), the EPR spectra of both paramagnetic species exhibit three well resolved

dx.doi.org/10.1021/ic400174r | Inorg. Chem. 2013, 52, 5246−5259

Table 5. Bond Distances (Å) and Angles (deg) Obtained for [M(no1pa2py)]$^+$ Complexes (M = Zn, Cu) with TPSSh/SVP Calculations in Aqueous Solution

	Λ(δδδ), Cu	Λ(δδδ), Zn		Δ(δδδ), Cu	Δ (δδδ), Zn
M−N1	2.377	2.339	M−N1	2.453	2.328
M−N2	2.069	2.217	M−N2	2.150	2.232
M−N3	2.174	2.263	M−N3	2.133	2.246
M−N4	2.056	2.097	M−N4	2.146	2.091
M−N5	2.077	2.183	M−N6	2.066	2.209
M−O1	2.009	2.086	M−O1	2.143	2.093
N1−M−N2	83.56	97.82	N1−M−N2	78.79	80.08
N1−M−N3	79.74	80.18	N1−M−N3	78.93	78.83
N1−M−N4	76.31	74.72	N1−M−N4	71.15	73.87
N1−M−N5	100.16	97.82	N1−M−N6	83.56	110.96
N1−M−O1	152.15	151.14	N1−M−O1	142.81	146.75
N2−M−N3	84.08	80.47	N2−M−N3	83.55	80.26
N2−M−N4	158.99	153.47	N2−M−N4	106.79	113.68
N2−M−N5	81.24	77.43	N2−M−N6	158.44	150.20
N2−M−O1	123.84	128.36	N2−M−O1	94.93	96.28
N3−M−N4	98.00	102.93	N3−M−N4	145.32	146.13
N3−M−N5	165.22	157.82	N3−M−N6	79.87	75.24
N3−M−O1	96.87	98.14	N3−M−O1	137.30	133.52
N4−M−N5	96.31	97.75	N4−M−N6	94.66	96.10
N4−M−O1	76.84	77.66	N4−M−O1	75.92	77.63
N5−M−O1	89.96	94.02	N6−M−O1	88.07	88.61

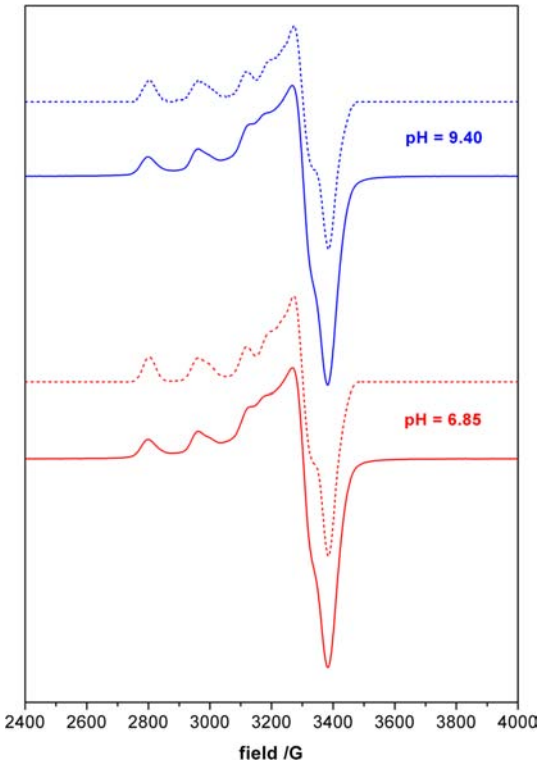

Figure 5. X-band EPR spectra of the complex of Cu^{2+} with H**no1pa2py** in aqueous solution at pH 6.85 and 9.40. Dashed lines represent the simulated spectra in each case.

lines of the four expected at low field from the coupling of the unpaired electron spin with the copper nucleus ($I = {}^3/_2$). The fourth line of both species is overlapped by the strong band at the high field part of the spectra. No superhyperfine splitting due to coupling with the nitrogen atoms of the ligand was observed. Spectroscopic visible data (λ_{max}), the hyperfine coupling constants A_i (i = x, y, and z), and the g values obtained by simulation of the spectra are compiled in Table 6.[36] These values indicate three different principal values for the g and A parameters of each species, with $g_z > (g_x + g_y)/2$ and the lowest g value ≥2.035, which is characteristic of mononuclear copper(II) complexes in $d_{x^2-y^2}$ ground state and elongation of the axial bonds. Elongated rhombic-octahedral, tetragonal, or distorted square pyramidal symmetries would be consistent with these data.[37] At the indicated pH, the percentages of the two species are 69% (A) and 31% (B). By increasing the pH to 9.40 no changes of the EPR parameters were observed, but the percentages of each species changed to 36% (A) and 64% (B). The two species exhibit quite different EPR parameters, with the A species presenting a higher g_z and a lower A_z than the B form.

Theoretical calculations of the g-tensors were performed with DFT on the Λ(δδδ) and Δ(δδδ) conformations of the [Cu(**no1pa2py**)]$^+$ complex described above. These calculations provided g_x = 2.083, g_y = 2.074, and g_z = 2.209 for the Λ(δδδ) form, and g_x = 2.077, g_y = 2.122, and g_z = 2.195 for the Δ(δδδ) isomer. On the basis of these data we assign the A and B species observed in the EPR spectrum to the Λ(δδδ) and Δ(δδδ) isomers, respectively. Our calculations appear to overestimate to a certain extent g_x and g_y, while g_z is slightly underestimated in the case of the Λ(δδδ) isomer. However, an overall good agreement is observed between the experimental and calculated g-values, which confirms that our DFT calculations provide molecular geometries in good agreement with the actual structure of the complex in solution.

Kinetic Inertness of the Copper(II) Complex of Hno1pa2py. A common method to ascertain the kinetic stability of metal complexes is the study of their acid-assisted dissociation. We have studied the dissociation of the copper(II) complex of H**no1pa2py** in aqueous solution under pseudo-first-order conditions by monitoring the decrease of the d−d transition band in the visible spectroscopic range. Due to the high inertness shown by the complex in preliminary assays, the conditions finally used to determine its half-life were in 3 M

dx.doi.org/10.1021/ic400174r | Inorg. Chem. 2013, 52, 5246−5259

Table 6. EPR Parameters for the Copper(II) Complexes of Hno1pa2py at 90 K in 1.0 M $NaClO_4$ Frozen Aqueous Solution[a]

		EPR parameters					
$[Cu(\mathbf{no1pa2py})]^+$	pH	g_x	g_y	g_z	A_x[b]	A_y[b]	A_z[b]
A expt	6.85	2.042	2.069	2.236	<5	9	160.4
$\Lambda(\delta\delta\delta)$ theor		2.083	2.074	2.209			
B expt	6.85	2.036	2.104	2.198	<5	11	191.2
$\Delta(\delta\delta\delta)$ theor		2.077	2.122	2.195			

[a]Complex concentration at *ca.* 2×10^{-3} M. [b]$A_i \times 10^4$ (cm^{-1}).

aqueous HCl at 90 °C. The half-life value ($t_{1/2}$) of 204 min (3.4 h) indicates a very high degree of kinetic inertness for the studied complex. Dissociation kinetics studies in acidic media are uncommon for complexes of Cu^{2+} with 1,4,7-triazacyclononane derivatives except for H_3nota, while being usual for complexes of cross-bridged derivatives of cyclen and cyclam such as H_2cb-do2a and H_2cb-te2a.[3] Half-lives have also been reported for complexes of monopicolinate derivatives of cyclen and cyclam, Hdompa and Htempa.[15] In Table 7 is shown a comparison of the reported half-lives for selected copper(II) complexes. Overall, and in spite of the various experimental conditions used, it is possible to conclude that the inertness of the complex of Cu^{2+} with H**no1pa2py** is clearly higher than those with Hdompa and Htempa and somewhat lower than that of [Cu(cb-te2a)], which is one of the most inert copper(II) complexes of polyaza ligands known.

Table 7. Acid-Assisted Dissociation Inertness of Selected Copper(II) Complexes

ligand	conditions	half-life ($t_{1/2}$), min	ref
Hno1pa2py	3 M HCl, 90 °C	204	this work
H_3nota	5 M HCl, 30 °C	<3	3
H_2cb-do2a	1 M HCl, 30 °C	240	3
H_2cb-te2a	5 M HCl, 90 °C	9240	3
Hdompa	2 M HCl, 25 °C	1.4	15
Htempa	1 M HCl, 25 °C	32	15

Electrochemistry of the Copper(II) Complex of Hno1pa2py. A relevant pathway for the dissociation of copper(II) complexes of macrocyclic ligands has been suggested to be the reduction to Cu^+ followed by demetalation of the complex.[1b] Thus, the electrochemical behavior of the copper(II) complex of H**no1pa2py** at neutral pH was studied by using cyclic voltammetry in aqueous solution (Figure 6). A quasireversible reduction system was observed at $E_{1/2}^{red} = -675$ mV versus Ag/AgCl, with a $\Delta E_p = 78$ mV ($E_{pc} = -714$ mV, $i_{pc} = 1.465 \times 10^{-5}$ A, $E_{pa} = -636$ mV, $i_{pa} = 1.368 \times 10^{-5}$ A). This result shows that the electrogenerated copper(I) complex is stable on the CV time scale, which demonstrates the capacity of H**no1pa2py** to adapt at least transiently to the copper(I) coordination requirements thus avoiding demetalation upon reduction of the metal ion. This is in contrast to the irreversible reduction found for complexes of most macrocyclic compounds including H_3nota, cyclen, cyclam, and H_2cb-do2a,[1b] while complexes of monopicolinate counterparts Hdompa and Htempa as well as of H_2cb-te2a present quasireversible reductions. The reduction process observed for the copper(II) complex of H**no1pa2py** ($E_{pc} = -518$ mV versus NHE, upon conversion) places it slightly outside the estimated −400 mV (NHE) threshold for typical bioreductants.[1b]

Copper-64 Radiolabeling. The high stability of the copper(II) complexes encouraged us to further examine the behavior of H**no1pa2py** with $^{64}Cu^{2+}$ following literature investigations.[4,38] Radiolabeling of H**no1pa2py** by copper-64 was investigated with solutions prepared as described in the Experimental Section. The "carrier added" solution was not obtained by addition of cold copper, but rather results from the presence of cold competitors [Cu (27.76%), Fe (14.30%), Ni (5.24%)] in the radioactive copper solution (specific activity: 2.32 GBq/μmol). The chelation was achieved at 6 < pH < 7, by reaction of solutions of $^{64}CuCl_2$ with H**no1pa2py** at 10, 1, and 0.1 mM concentrations in 0.1 M ammonium acetate. Reaction mixtures were stirred at room temperature during 5, 15, and 30 min, and radiolabeled solutions were analyzed on TLC plates and by means of HPLC experiments. No H**no1pa2py** concentration lower than 0.1 mM was investigated since at this concentration the specific radiolabeling activity of 364 MBq/μmol was already quite low for an application in immunodiagnostic. This result has to be associated with the specific activity of the copper solution as described above. A great improvement will be reached when higher copper-64 specific activity solutions are used.

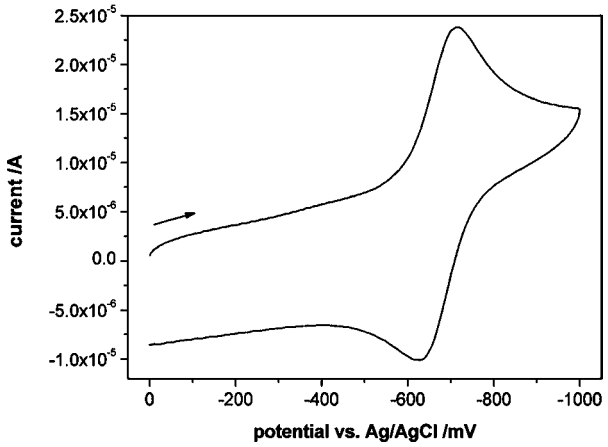

Figure 6. Cyclic voltammogram of $[Cu(\mathbf{no1pa2py})]^+$ in aqueous solution at neutral pH recorded at 100 mV s^{-1}.

Thin layer radiochromatograms, which present the measured radioactive emission on a storage phosphor screen after 30 min incubation time, are presented in Figure 7 (see Supporting Information, Figure S5, for 5 and 15 min). In each case, free $^{64}Cu^{2+}$ was not observed, and an outstanding 100% radiolabeling of H**no1pa2py** with $^{64}Cu^{2+}$ was observed. Three radiolabeled species with different abundances (~60% + 25% + 15%) were observed for all incubation times.

The HPLC radiochromatogram obtained from a 1 mM ligand solution after a 30 min of incubation time is compared to that of ^{64}Cu-acetate as a reference in Figure 8 (chromatograms B and C). The diagrams confirm the results initially obtained on TLC plates, showing that three radiolabeled species are formed in comparable ratios, while free ^{64}Cu was not detected.

dx.doi.org/10.1021/ic400174r | Inorg. Chem. 2013, 52, 5246−5259

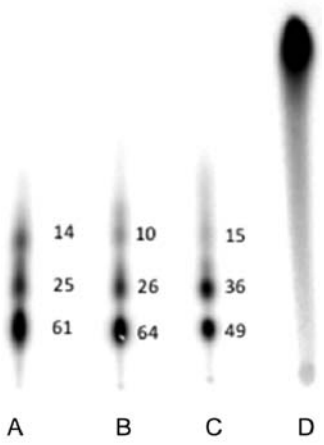

Figure 7. Thin layer radiochromatogram of $[^{64}Cu(\mathbf{no1pa2py})]^+$ and % of ^{64}Cu emission: (A) 10 mM ligand and 30 min incubation time; (B) 1 mM ligand and 30 min incubation time; (C) 0.1 mM ligand and 30 min incubation time; (D) copper-64 acetate as reference.

The same experiment was then performed with the "cold" complex $[Cu(\mathbf{no1pa2py})]^+$, and the equivalent UV-HPLC chromatogram obtained is also presented in Figure 8 (chromatogram A). It showed two major species with relative abundances of 72% (lower R_f) and 29% (higher R_f), indicating that the third species observed upon ^{64}Cu complexation is related to side effects of the radiolabeling technique, for instance radiolysis phenomena associated to the radiation emitted by copper-64. Indeed, ionizing radiation generates radical species, including $OH^{\bullet}$, which can react with the copper complex and explain the formation of hydroxide species even at neutral pH values.[39] Even so, the HPLC chromatograms shown in Figure 8 indicate the presence of two complex species when using cold Cu^{2+}. The presence of several ^{64}Cu radiolabeled species has been previously observed for other polyazamacrocycles, and attributed to the formation of dimers or the presence of impurities.[40] The formation of three different radiolabeled species may reflect the coordination versatility of the ligand: first of all, the macrocycle can act as a N_5O or N_6 donor; additionally, Jahn–Teller effects may result in 4 or 5-coordinate copper centers (as previously seen in the crystal structure of the methyl ester derivative). The crystal structure of $[Cu(H\mathbf{L1})Cl]^+$ also revealed that coordinating anions can also participate in the primary coordination sphere. Therefore, a large excess of acetate in the experimental workup could also result in the formation of ternary complexes with this anion and such effect has to be considered.

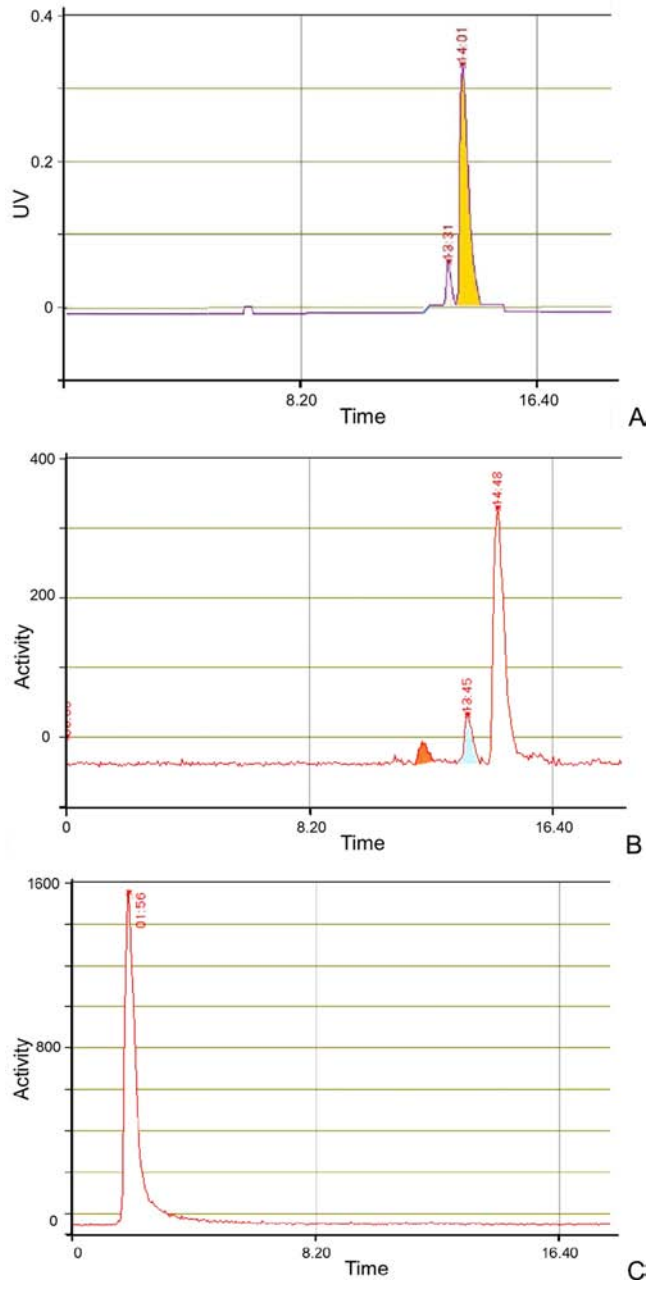

Figure 8. (A) HPLC UV-chromatogram of $[Cu(\mathbf{no1pa2py})]^+$. (B) HPLC radiochromatogram of 1 mM H**no1pa2py** labeled with $^{64}Cu^{2+}$ (30 min incubation time). (C) HPLC radiochromatogram of copper-64 acetate.

CONCLUSIONS

Macrocyclic chelators and their metal complexes have widespread applications in the biomedical sciences, including radiopharmaceutical chemistry. The use of copper radionuclides in radiopharmaceuticals is increasing, and the challenge still persists to develop new chelators able to meet the very strict metal binding specifications for applications such as PET imaging or radiotherapy. Picolinate groups appended on macrocycles proved to yield efficient chelators for copper(II). In this work we have presented the synthesis of a new ligand, **Hno1pa2py**, based on the tacn framework functionalized with two picolyl and one picolinate pendant arms, and designed for stable complexation of Cu^{2+} ions in aqueous solution. Selective *N*-functionalization of the macrocyclic backbone was obtained following an easy-to-run procedure involving orthoamide chemistry. The final chelator was obtained in a six-step procedure with good overall yields. The ligand exhibits a low overall basicity due to the small macrocyclic cavity and the introduction of aromatic groups. The copper(II) complexation process was found to be very fast, including in acid medium. Besides, the thermodynamic stability of the complexes of Cu^{2+} was found to be relatively high compared to other tacn-based ligands, and the pCu value showed high selectivity of **Hno1pa2py** for Cu^{2+} over Zn^{2+}. A detailed investigation of the structure of the complexes by using EPR and UV–vis spectroscopies and ^1H and ^{13}C NMR experiments at variable temperatures, supported by additional DFT calculations, indicates that at neutral pH the complex is

dx.doi.org/10.1021/ic400174r | Inorg. Chem. 2013, 52, 5246–5259

present in solution as a mixture of two isomers: $\Lambda(\delta\delta\delta)$ and $\Delta(\delta\delta\delta)$. The two isomers present very distorted octahedral coordination environments in which the ligand uses a N_5O donor set, with one of the picolyl pendant arms remaining uncoordinated.

The investigation of the kinetic stability of the complexes in acidic solutions underlines a high kinetic inertness of the $[Cu(\mathbf{no1pa2py})]^+$ complex compared to other copper(II) complexes of macrocyclic ligands reported in the literature. In addition, CV experiments performed in aqueous solution confirmed its inertness by emphasizing a good stability of the complexes upon reduction of the metal ion to Cu^+ at neutral pH.

The H**no1pa2py** ligand consequently appears as a very attractive candidate for the design of Cu^{2+}-based radiopharmaceuticals for application in PET imaging and encouraged us to investigate, as a preliminary study, the ability of this ligand to chelate the ^{64}Cu radionuclide. Radiolabeling with ^{64}Cu was demonstrated to be very efficient with a quantitative complexation of the hot metal. Thus, this ligand scaffold is promising for the preparation of chelates for PET applications provided that the minor species observed in solution can be separated, for instance by HPLC workup.

EXPERIMENTAL SECTION

Materials and Methods. Reagents were purchased from ACROS Organics and from Aldrich Chemical Co. 1,4,7-Triazacyclononane (tacn) was purchased from CheMaTech (Dijon, France). 6-Chloromethylpyridine-2-carboxylic acid methylester was synthesized according to a published method.[25] Acetonitrile, toluene, and water solvents were distilled before use. Elemental analyses were performed at the Service de Microanalyse, CNRS, 69360 Solaize, France. NMR and MALDI mass spectra were recorded at the "Services communs" of the University of Brest. ^1H and ^{13}C NMR spectra were recorded with Bruker Avance 500 (500 MHz), Bruker Avance 400 (400 MHz), or Bruker AMX-3 300 (300 MHz) spectrometers; NMR spectra of all the previously described derivatives are given in the Supporting Information (Figures S6–S10). MALDI mass spectra were recorded with an Autoflex MALDI TOF III LRF200 CID spectrometer.

1,4-Bis(pyridin-2-ylmethyl)-1,4,7-triazacyclononane (5). *N*-Dimethoxymethyl-*N*,*N*-dimethylamine (910 μL, 6.8 mmol, 1.1 equiv) was added to a solution of tacn (880 mg, 6.81 mmol) in chloroform (2 mL) and toluene (8 mL) The reaction mixture was heated to reflux with stirring for 2 h, and then the solvent was evaporated under reduced pressure yielding a clear oil. This crude product was dissolved in acetonitrile (20 mL) and added dropwise to a solution of 2-chloromethylpyridine (950 mg, 7.48 mmol, 1.1 equiv) in acetonitrile (50 mL). The reaction mixture was stirred at room temperature (rt) for one week, and then the solvent was evaporated under reduced pressure to yield a brown powder, which was dissolved in water and stirred at reflux during 3 h. The solvent was evaporated under reduced pressure yielding a brown oil, which was dissolved in acetonitrile (20 mL). A solution of 2-chloromethylpyridine (950 mg, 7.48 mmol, 1.1 equiv) in acetonitrile (20 mL) and potassium carbonate (2.5 equiv) were added. The mixture was stirred at rt for 4 days and filtered, and the solvent was evaporated under reduced pressure to yield a brown oil. The resulting product was dissolved in methanol (30 mL), hydrochloric acid (6 M, 30 mL) was added, and the mixture was refluxed with stirring during 3 h. Distilled water was added (40 mL), and the solution was extracted with chloroform (40 mL). The pH of the aqueous layer was adjusted to ~12 with NaOH pellets, and then extracted with chloroform (3 × 50 mL). Organic layers were recombined, dried under $MgSO_4$, and filtered. The filtrate was evaporated under reduced pressure yielding a brown oil. The residue was purified by column chromatography using neutral alumina ($CHCl_3$/MeOH 95/5) to yield **5** as a brown oil (1.99 g, 60%). ^1H NMR ($CDCl_3$, 400 MHz): 2.51 (m, 8 H, tacn); 2.62 (m, 4 H, m, tacn); 3.74 (s, 4 H, CH_2-py); 6.99 (dd, 2 H, ^3J = 6.6 Hz, ^3J = 4.9 Hz, H_{arom}); 7.36 (d, 2 H, ^3J = 7.6 Hz, H_{arom}); 7.47 (dd, 2 H, ^3J = 7.6 Hz, ^3J = 6.6 Hz, H_{arom}); 8.37 (d, 2 H, ^3J = 4.9 Hz, H_{arom}). ^{13}C NMR ($CDCl_3$, 100 MHz): δ 46.3, 51.5, 52.4 (tacn); 63.0 (CH_2-py); 121.6, 122.8, 136.0, 148.6 (C_{arom}); 159.9 (C_q).

1-Methylpicolinate-4,7-bis(pyridin-2-ylmethyl)-1,4,7-triazacyclononane (L1). Sodium carbonate (88 mg, 0.8 mmol) and a solution of 6-chloromethylpyridine-2-carboxylic acid methylester (62 mg, 0.3 mmol) in acetonitrile (10 mL) were added to a solution of **5** (100 mg, 0.3 mmol), and the mixture was stirred at 50 °C for 3 days. After cooling, the solution was filtered and the filtrate evaporated under vacuum. The residue was purified by column chromatography using neutral alumina ($CHCl_3$/MeOH 98/2), yielding a brown oil (137 mg, 93%). ^1H NMR ($CDCl_3$, 400 MHz): 2.86 (s, 12 H, tacn); 3.80 (s, 4 H, CH_2-py); 3.92 (s, 2 H, CH_2-pic); 3.95 (s, 3 H, CH_3); 7.11 (dd, 2 H, ^3J = 4.8 Hz, ^3J = 7.4 Hz, $H_{arom\text{-}py}$); 7.46 (d, 2 H, ^3J = 7.6 Hz, $H_{arom\text{-}py}$); 7.61 (t, 2 H, ^3J = 7.6 Hz, $H_{arom\text{-}py}$); 7.78–7.76 (m, 2 H, $H_{arom\text{-}pic}$); 7.96 (dd, 1 H, ^3J = 3.6 Hz, ^3J = 5.2 Hz, $H_{arom\text{-}pic}$); 8.47 (d, 2 H, ^3J = 4.8 Hz, $H_{arom\text{-}py}$). ^{13}C NMR ($CDCl_3$, 100 MHz): 52.8 (CH_3); 55.8 (tacn); 64.6 (CH_2); 121.8, 123.1 ($C_{arom\text{-}py}$); 123.4, 126.4 ($C_{arom\text{-}pic}$); 136.2 ($C_{arom\text{-}py}$); 137.1 ($C_{arom\text{-}pic}$); 147. 0 (C_q-CO_2CH_3); 148.8 ($C_{arom\text{-}py}$); 160.3, 161.4 (C_q-CH_2); 165.9 (CO_2CH_3). MALDI-TOF: m/z 461.2 $[M + 1]^+$; 462.2 $[M + 2]^+$; 463.2 $[M + 3]^+$.

1-Picolinic Acid-4,7-bis(pyridin-2-ylmethyl)-1,4,7-triazacyclononane Hydrochloride (Hno1pa2py). A solution of **L1** (570 mg, 1.24 mmol) in hydrochloric acid (6 M, 10 mL) was stirred at 55 °C for 2 days, and then evaporated under reduced pressure. Addition of diethyl ether lead to precipitation of the desired compound as an off-white powder (776 mg, 94%). ^1H NMR (D_2O, 400 MHz): 2.89 (s, 4 H, tacn); 2.91 (bs, 4 H, tacn); 3.42 (bs, 4 H, tacn); 4.16 (s, 4 H, CH_2-py); 4.61 (s, 2 H, CH_2-pic); 7.83 (d, 1 H, ^3J = 7.6 Hz, $H_{arom\text{-}pic}$); 7.89 (dd, 2 H, ^3J = 6.6 Hz, $H_{arom\text{-}py}$); 8.06 (d, 2 H, ^3J = 8.0 Hz, $H_{arom\text{-}py}$); 8.18 (t, 1 H, ^3J = 7.6 Hz, $H_{arom\text{-}pic}$); 8.31 (d, 1 H, ^3J = 7.6 Hz, $H_{arom\text{-}pic}$); 8.48 (dd, 2 H, ^3J = 6.6 Hz, ^3J = 8.0 Hz, $H_{arom\text{-}py}$); 8.56 (d, 2 H, ^3J = 6.6 Hz, $H_{arom\text{-}py}$). ^{13}C NMR (D_2O, 100 MHz): 47.5, 52.8, 54.2 (tacn); 58.0 (CH_2-py); 61.2 (CH_2-pic); 129.2, 130.7 ($C_{arom\text{-}pic}$); 129.5, 132.1 ($C_{arom\text{-}py}$); 143.6, 144.3 ($C_{arom\text{-}py}$); 150.2, 150.8 ($C_{arom\text{-}pic}$); 153.4, 154.3 ($C_{q\text{-}arom}$); 170.3 (C_q-CO_2H). MALDI-TOF: m/z 447.2 $[M + 1^+]$. Anal. Calcd for $C_{25}H_{30}N_6O_2{\cdot}6HCl{\cdot}2H_2O$: C, 42.81; H, 5.75; N, 11.98. Found: C, 42.57; H, 5.72; N, 11.73.

Caution! *Although no problem was found during our experiments, salts of perchlorate and their metal complexes are potentially explosive and should be handled with great care and in small quantities.*

Preparation of [CuL1](ClO$_4$)$_2$]. $Cu(ClO_4)_2{\cdot}6H_2O$ (40 mg, 0.108 mmol) was added to a solution of **Hno1pa2py** (50 mg, 0.108 mmol) in water (5 mL), and the pH of the solution was adjusted to ≈4.5 with an aqueous HCl solution (1 M). The mixture was heated at 40 °C during 14 h. The solution was evaporated; the resulting blue solid dissolved in a minimum quantity of methanol, and diethylether was added. The precipitate formed was filtered to yield a turquoise powder. Single crystals suitable for X-ray diffraction analysis were obtained upon slow evaporation of an aqueous solution of the turquoise powder (73 mg, 83%). Anal. Calcd for $C_{26}H_{32}Cl_2CuN_6O_{10}{\cdot}1.5H_2O{\cdot}KCl$: C, 34.73; H, 3.92; N, 9.35. Found: C, 34.75; H, 3.88; N, 8.85.

Preparation of [Cu(no1pa2py)](ClO$_4$). $Cu(ClO_4)_2{\cdot}6H_2O$ (100 mg, 0.270 mmol) was added to a solution of H**no1pa2py**·6HCl·2H$_2$O (185 mg, 0.265 mmol) in water (25 mL). The solution was slowly neutralized by addition of diluted aqueous KOH, and then stirred at rt overnight. The turquoise solution obtained was evaporated and dried under vacuum, the residue was taken in 25 mL of dry MeCN, and the colorless insoluble matter was separated by filtration. This isolation procedure was repeated 3 times in progressively smaller volumes of dry MeCN until no more inorganic matter separated. The clear solution was then evaporated and dried under vacuum to yield a turquoise solid (146 mg, 88%). Anal. Calcd for $C_{25}H_{29}ClCuN_6O_6{\cdot}0.5CH_3CN$: C, 49.64; H, 4.89; N, 14.47. Found: C, 49.90; H, 5.26; N, 14.54. Selected IR bands (KBr, cm^{-1}): $\nu_{as}(COO^-)$ 1635 (s) and 1598 (s), $\nu_s(COO^-)$ 1381 (m); ν(Cl–O) (ClO_4^-) centered at 1100 (vs).

dx.doi.org/10.1021/ic400174r | Inorg. Chem. 2013, 52, 5246–5259

X-ray Diffraction Studies. X-ray diffraction data were collected with a circular diffractometer X-Calibur-2 CCD 4 (OXFORD DIFFRACTION), including a four circle goniometer (KM4) and a two-dimensional CCD detector (SAPPHIRE 2). Three dimensional X-ray diffraction data were collected on an X-CALIBUR-2 CCD 4-circle diffractometer (Oxford Diffraction). Data reduction, including interframe scaling, Lorentz, polarization, empirical absorption, and detector sensitivity corrections, was carried out using attached programs of Crysalis software[41] (Oxford Diffraction). Complex scattering factors were taken from the program SHELX97[42] running under the WinGX program system.[43] The structure was solved by direct methods with SIR-97[44] and refined by full-matrix least-squares on F^2. All hydrogen atoms were included in calculated positions and refined in riding mode. Crystal data and details on data collection and refinement are summarized in Table 8. CCDC 919095 and 919096 contain the supplementary crystallographic data for this Article. These data can be obtained free of charge from the Cambridge Crystallographic Data Centre via www.ccdc.cam.ac.uk/data_request/cif.

Table 8. Crystal Data and Refinement Details for $[CuL1](ClO_4)_2\cdot H_2O$

	$[CuL1](ClO_4)_2\cdot H_2O$
formula	$C_{26}H_{34}Cl_2CuN_6O_{11}$
MW	741.03
cryst syst	monoclinic
space group	$P2_1/c$
T/K	170(2)
a/Å	8.5089(2)
b/Å	22.8400(18)
c/Å	15.8525(3)
α/deg	90
β/deg	90.901(2)
γ/deg	90
V/Å^3	3080.4(3)
F(000)	1532
Z	4
λ, Å (Mo Kα)	0.710 73
D_{calc}/g cm^{-3}	1.598
μ/mm^{-1}	0.952
θ range/deg	2.84–28.28
R_{int}	0.0204
reflns measd	26 979
unique reflns	7636
reflns obsd	6270
GOF on F^2	1.027
R1[a]	0.0522
wR2 (all data)[b]	0.1444
largest differences peak and hole/e Å^{-3}	1.054 and −0.645

[a] $R1 = \sum||F_o| - |F_c||/\sum|F_o|$. [b] $wR2 = \{\sum[w(|F_o|^2 - |F_c|^2)^2]/\sum[w(F_o^4)]\}^{1/2}$.

Computational Details. All calculations presented in this work were performed employing the Gaussian 09 package (Revision B.01).[45] Full geometry optimizations of the $[CuL1]^{2+}$, $[Cu(\mathbf{no1pa2py})]^+$, and $[Zn(\mathbf{no1pa2py})]^+$ complexes were performed in aqueous solution employing DFT within the hybrid meta-GGA approximation with the TPSSh exchange-correlation functional.[46] Input geometries were generated from the crystallographic data of $[CuL1](ClO_4)_2$. For geometry optimization purposes we used the standard Ahlrich's valence double-ξ basis set with polarization functions (SVP).[47] No symmetry constraints have been imposed during the optimizations. In the case of copper complexes calculations were performed by using an unrestricted model, and therefore spin contamination[48] was assessed by a comparison of the expected difference between $S(S+1)$ for the assigned spin state [$S(S+1) = 0.75$ for the mononuclear copper(II) complexes investigated here] and the actual value of $\langle S^2\rangle$.[49] The results obtained indicate that spin contamination is negligible for systems investigated in this work [$\langle S^2\rangle - S(S+1) < 0.0020$]. The stationary points found on the potential energy surfaces as a result of geometry optimizations were tested to represent energy minima rather than saddle points via frequency analysis. The default values for the integration grid (75 radial shells and 302 angular points) and the SCF energy convergence criteria (10^{-8}) were used in all calculations. The relative free energies of the different conformations of $[Cu(\mathbf{no1pa2py})]^+$ and $[Zn(\mathbf{no1pa2py})]^+$ complexes were calculated in aqueous solution at the TPSSh/SVP level, and they include non-potential-energy contributions (zero point energies and thermal terms) obtained through frequency analysis.

Throughout this work solvent effects were included by using the polarizable continuum model (PCM), in which the solute cavity is built as an envelope of spheres centered on atoms or atomic groups with appropriate radii. In particular, the integral equation formalism (IEFPCM) variant as implemented in Gaussian 09 was used.[50]

Calculation of EPR parameters (g-tensor) was performed in aqueous solution with the TPSSh functional. In these calculations we used the aug-cc-pVTZ-J basis set of Sauer for Cu,[51] and for the C, H, N, and O atoms we used the EPR-III basis sets of Barone,[52] which is a triple-ζ basis set including diffuse functions, double d-polarizations, and a single set of f-polarization functions, together with an improved s-part to better describe the nuclear region. The g-tensor was calculated as a correction, Δg, to the free electron g-value (g_e = 2.002 3193) that represents contributions of three gauge including atomic orbitals (GIAO) magnetic shielding terms:

$$\Delta g = g_e + g_{RMC} + g_{DC} + g_{OZ/SOC}$$

Here g_{RMC} is the relativistic mass correction, g_{DC} is the diamagnetic correction, and $g_{OZ/SOC}$ represents the orbital Zeeman and spin−orbit coupling contributions.[53]

Potentiometric Studies. *Equipment and Work Conditions.* The potentiometric setup consisted of a 50 mL glass-jacketed titration cell sealed from the atmosphere and connected to a separate glass-jacketed reference electrode cell by a Wilhelm type salt bridge filled with 0.1 M KNO_3 electrolyte. An Orion 720A+ measuring instruments fitted with a Metrohm 6.0123.100 glass electrode and a Metrohm 6.0733.100 Ag/AgCl reference electrode was used for the measurements. The ionic strength of the experimental solutions was kept at 0.10 ± 0.01 M with KNO_3; temperature was controlled at 298.2 ± 0.1 K using a Huber CC3-K6 compact cooling and heating bath thermostat and a previously calibrated Orion 91-70-06 ATC-probe. Atmospheric CO_2 was excluded from the titration cell during experiments by slightly bubbling purified nitrogen on the experimental solution. Titrant solutions were added through capillary tips at the surface of the experimental solution by a Metrohm Dosimat 665 automatic buret. Titration procedure is automatically controlled by software after selection of suitable parameters, allowing for long unattended experimental runs. The titrant was a KOH solution prepared at *ca.* 0.1 M from a commercial ampule of analytical grade, and its accurate concentration was obtained by application of the Gran's method[54] upon titration of a standard HNO_3 solution. Ligand solutions were prepared at *ca.* 2.0×10^{-3} M, and the Cu^{2+} and Zn^{2+} solutions were prepared at *ca.* 0.05 M from analytical grade nitrate salts and standardized by complexometric titrations with H_4edta (ethylenediaminetetraacetic acid).[55] Sample solutions for titration contained approximately 0.04 mmol of ligand in a volume of 30.00 mL. In complexation titrations metal cations were added at 0.9 equiv of the ligand amount. In competition titrations H_4edta was additionally added at 1.2 equiv.

Measurements. The electromotive force of the sample solutions was measured after calibration of the electrode by titration of a standard HNO_3 solution at 2.0×10^{-3} M in the work conditions. The $[H^+]$ of the solutions was determined by measurement of the electromotive force of the cell, $E = E^{o\prime} + Q \log [H^+] + E_j$. The term pH is defined as $-\log[H^+]$. $E^{o\prime}$ and Q were determined by acid region of the calibration curves. The liquid-junction potential, E_j, was found

dx.doi.org/10.1021/ic400174r | Inorg. Chem. 2013, 52, 5246−5259

to be negligible under the experimental conditions used. The value of $K_w = [H^+][OH^-]$ was found to be equal to $10^{-13.78}$ by titrating a solution of known hydrogen-ion concentration at the same ionic strength in the alkaline pH region, considering $E^{\circ\prime}$ and Q valid for the entire pH range. The protonation constants of H_4edta and the thermodynamic stability constants of its copper(II) complex used in competition titration refinements were taken from the literature.[34] Each titration consisted of 50−70 equilibrium points in the range pH 2.5−11.5, and at least two replicate titrations were performed for each particular system. Backtitrations were always performed at the end of each direct complexation titration in order to check if equilibrium was attained throughout the full pH range.

Calculations. The potentiometric data were refined with the HYPERQUAD software,[56] and speciation diagrams were plotted using the HySS software.[57] The overall equilibrium constants β_i^H and $\beta_{M_mH_hL_l}$ are defined by $\beta_{M_mH_hL_l} = [M_mH_hL_l]/[M]^m[H]^h[L]^l$ ($\beta_i^H = [H_hL_l]/[H]^h[L]^l$ and $\beta_{MH_{-1}L=} \beta_{ML(OH)} \times K_w$). Differences, in log units, between the values of protonated (or hydrolyzed) and nonprotonated constants provide the stepwise (log K) reaction constants (being $K_{M_mH_hL_l} = [M_mH_hL_l]/[M_mH_{h-1}L_l][H]$). The errors quoted are the standard deviations calculated by the fitting program from all the experimental data for each system.

Spectroscopic Studies. A stock solution of the complex of H**no1pa2py** with Cu^{2+} was prepared at 2.86×10^{-3} M. The spectra in the visible region were measured on a Unicam UV4 spectrometer in aqueous solutions at 298 K. Sample solutions of the complex were measured at pH 1.95, 6.85, and 9.40, after adjustment by addition of KOH or HNO_3. EPR spectra were recorded on a Bruker EMX 300 spectrometer operating at the X-band and equipped with a continuous-flow cryostat for liquid nitrogen. Sample solutions of the complex at *ca.* 2.0×10^{-3} M and 1 M in $NaClO_4$ were prepared at pH values of 1.90, 2.41, 3.00, 6.85, and 9.40 by addition of aqueous $NaClO_4$ to the stock solution followed by pH adjustment with HNO_3 or KOH (see Figure S6 of the Supporting Information). The EPR spectra of the frozen solutions at 90 K were recorded at an attenuated microwave power of 2.0 mW and a microwave frequency of 9.5 GHz. Experimental EPR spectra were simulated using the SpinCount software[36] to determine the relevant parameters. The infrared spectrum (400−4000 cm^{-1}) of the [Cu(**no1pa2py**)](ClO_4) complex was acquired on a Bruker IFS 66/S spectrometer as a KBr pellet.

Electrochemical Studies. Cyclic voltammograms were performed in aqueous solution at rt with a BAS CV-50W voltammetric analyzer operated with BAS data acquisition software. Experiments were run in a glass cell BAS MF-1082 placed inside a BAS C-2 cell stand (Faraday cage). The three-electrode setup consisted of a reference Ag/AgCl electrode (BAS MF-2052) filled with aqueous 3 M NaCl solution, a platinum wire auxiliary electrode (BAS MW-1032), and a glassy carbon working electrode (BAS MF-2012). A solution of the Cu^{2+} complex of HL2 at neutral pH was prepared at 1.43×10^{-3} M in 0.10 M NMe_4NO_3 electrolyte. Sample solutions were degassed by bubbling N_2 prior to all measurements, and were kept under a N_2 stream during the measurements. Between each scan the working electrode was electrocleaned by multicycle scanning in the supporting electrolyte solution, polished on alumina 1 and 0.05 μm, cleaned with water and sonicated before use, according to standard procedures. Cyclic voltammograms with sweep rate ranging from 10 to 200 mV s^{-1} were recorded in the region from 0 to −1000 mV, with the voltage being ramped from 0 to −1000 mV and then back to 0 mV. At this potential range the ligand was found to be electroinactive. The half-wave potentials, $E_{1/2}$'s, were obtained by averaging the anodic and cathodic peak potentials. All potential values are reported relative to the Ag/AgCl reference electrode in aqueous 3 M NaCl unless otherwise noted.

Kinetic Inertness of the Complex of Cu^{2+} in Acidic Media (HCl). The measurement of the acid-assisted dissociation of the complex of Cu^{2+} with H**no1pa2py** was performed under pseudo-first-order conditions by addition of concentrated aqueous solutions of HCl to an aqueous solution of the preformed complex at *ca.* 2×10^{-3} M. Dissociation was followed by the decrease with time in the intensity of the d−d transition band of the complex in the visible range at 660 nm, at 90 °C and 3 M HCl without control of ionic strength. The experimental data were fitted by exponential regression, after correction for background absorbance due to the weakly absorbing free Cu^{2+} in the presence of excess Cl^- anions, in order to calculate the half-life of the complex.

Copper-64 Radiolabeling. Copper-64 dichloride in 0.1 M hydrochloric acid was obtained from the ARRONAX cyclotron (Saint-Herblain, France). Radiochemical purity was determined by gamma spectroscopy, and chemical purity was controlled by ICP-OES. For radiolabeling solutions, ammonium acetate, hydrochloric acid 30%, and sodium hydroxide pellets were purchased as trace select grade from Fluka Analytical. Ammonium chloride ACS reagent (Sigma-Aldrich), methanol HPLC grade (Fisher Chemical), and acetonitrile gradient grade (Fisher Scientific) were used for the analytical controls. Water (18.2 MΩ cm) for aqueous solutions was obtained from a Milli-Q gradient system (Millipore). **Hno1pa2py** copper-64 chelation was achieved by addition of 5 μL carrier-added $^{64}CuCl_2$ solution (1.8 MBq, 11.5 ppm of total copper for 44 ppm total metal, specific activity of 2.32GBq/μmol), and 5 μL of 0.1 M sodium hydroxide to 50 μL of H**no1pa2py** solutions in 0.1 M ammonium acetate at different concentration levels (10 mM; 1 mM; 0.1 mM). Reaction mixtures were stirred at rt for 5, 15, and 30 min, and radiolabeled solutions were analyzed on TLC plates (silica gel on TLC-PET foils, Fluka analytical) and HPLC. A mixture of ammonium chloride (20% in water) and methanol (1:1) was used for TLC analyses. TLC plates were revealed on a storage phosphor screen using a Cyclone Plus phosphor imager (Perkin-Elmer). HPLC analyses were performed using an Eckert & Ziegler HPLC Module, Knauer pumps K120, Knauer HPLC Degasser, and a reverse phase HPLC column (ACE C18.3 μm, 150 mm × 3 mm) with the following elution gradient: isocratic mode ammonium acetate buffer (50 mM, pH 4.5) during 2.5 min; then addition of acetonitrile from 0 to 10% in the ammonium acetate buffer, for 15 min at a flow rate of 0.5 mL/min; and finally 10% of acetonitrile during 2.5 min. Radioactive and UV (227 nm) profiles were monitored with an Eckert & Ziegler detector shielding module and a Knauer smartline UV 2520 using Modular-Lab software.

■ ASSOCIATED CONTENT

Ⓢ Supporting Information

Structure, bond distances, angles, and description of the structure of complex [Cu(H**L1**)Cl]$(ClO_4)_2 \cdot H_2O$ (**7**) obtained at pH 1.5. X-ray crystal structures of [Cu**L1**]$(ClO_4)_2 \cdot H_2O$ (**6**) and [Cu(H**L1**)Cl]$(ClO_4)_2 \cdot H_2O$ (**7**) in CIF format. NMR spectra (^1H and ^{13}C) of precursors and ligands **L1** and H**no1pa2py**. ^1H and ^{13}C NMR spectra of $[Zn(no1a2py)]^+$ at different temperatures, X-band EPR spectra of the complex of Cu^{2+} with H**no1pa2py**, experimental (X-ray) and calculated (UTPSSh/SVP) bond lengths (Å) and angles (deg) of the metal coordination environment in $[Cu\mathbf{L1}]^{2+}$, and TLC experiments with ^{64}Cu. This material is available free of charge via the Internet at http://pubs.acs.org.

■ AUTHOR INFORMATION

Corresponding Author

*E-mail: carlos.platas.iglesias@udc.es (C.P.-I); delgado@itqb.unl.pt (R.D.); raphael.tripier@univ-brest.fr (R.T.).

Notes

The authors declare no competing financial interest.

■ ACKNOWLEDGMENTS

R.T. acknowledges the Ministère de l'Enseignement Supérieur et de la Recherche, the Centre National de la Recherche Scientifique, the ANR program αRIT/βPET, and especially the financial support from the Région Bretagne, France. R.T. also

thanks the "Service Commun" of NMR facilities of the University of Brest. C.P.-I. acknowledges Centro de Supercomputación de Galicia (CESGA) for providing the computer facilities. R.D. and L.M.P.L. acknowledge Fundação para a Ciência e a Tecnologia (FCT), with coparticipation of the European Community funds FEDER, POCI, QREN, and COMPETE for the financial support under Project PTDC/QUI/67175/2006. L.M.P.L. thanks FCT also for a postdoctoral fellowship (SFRH/BPD/73361/2010).

REFERENCES

(1) (a) Smith, S. V. *J. Inorg. Biochem.* **2004**, *98*, 1874−1901. (b) Shokeen, M.; Anderson, C. J. *Acc. Chem. Res.* **2009**, *42*, 832−841.
(2) (a) Liu, W.; Hao, G.; Long, M. A.; Anthony, T.; Hsieh, J.-T.; Sun, X. *Angew. Chem., Int. Ed.* **2009**, *48*, 7346−7349. (b) Boswell, C. A.; Regino, C. A. S.; Baidoo, K. E.; Wong, K. J.; Bumb, A.; Xu, H.; Milenic, D. E.; Kelley, J. A.; Lai, C. C.; Brechbiel, M. W. *Bioconjugate Chem.* **2008**, *19*, 1476−1484. (c) Sprague, J. E.; Peng, Y.; Fiamengo, A. L.; Woodin, K. S.; Southwick, E. A.; Weisman, G. R.; Wong, E. H.; Golen, J. A.; Rheingold, A. L.; Anderson, C. J. *J. Med. Chem.* **2007**, *50*, 2527−2535. (d) Cooper, M. S.; Ma, M. T.; Sunassee, K.; Shaw, K. P.; Williams, J. D.; Paul, R. L.; Donnelly, P. S.; Blower, P. J. *Bioconjugate Chem.* **2013**, *23*, 1029−1039. (e) Juran, S.; Wather, M.; Stephan, H.; Bergmann, R.; Steinbach, J.; Kraus, W.; Emmerling, F.; Comba, P. *Bioconjugate Chem.* **2009**, *20*, 347−359. (f) Christine, C.; Koubemba, M.; Shakir, S.; Clavier, S.; Ehret-Sabatier, L.; Saupe, F.; Orend, G.; Charbonniere, L. J. *Org. Biomol. Chem.* **2012**, *10*, 9183−9190.
(3) Wadas, T. J.; Wong, E. H.; Weisman, G. R.; Anderson, C. J. *Chem. Rev.* **2010**, *110*, 2858−2902.
(4) Pandya, D. N.; Dale, A. V.; Kim, J. Y.; Lee, H.; Ha, Y. S.; An, G. I.; Yoo, J. *Bioconjugate Chem.* **2012**, *23*, 330−335.
(5) (a) Bartholomä, M. D. *Inorg. Chim. Acta* **2012**, *389*, 36−51. (b) Mewis, R. E.; Archibald, S. J. *Coord. Chem. Rev.* **2010**, *254*, 1686−1712.
(6) Anderegg, A.; Arnaud-Neu, F.; Delgado, R.; Felcman, J.; Popov, K. *Pure Appl. Chem.* **2005**, *77*, 1445−1495.
(7) Maheshwari, V.; Dearling, J. L. J.; Treves, S. T.; Packard, A. B. *Inorg. Chim. Acta* **2012**, *393*, 318−323.
(8) Bass, L. A.; Wang, M.; Welch, M. J.; Anderson, C. J. *Bioconjugate Chem.* **2000**, *11*, 527−532.
(9) (a) Sargeson, A. M. *Coord. Chem. Rev.* **1996**, *151*, 89−114. (b) Di Bartolo, N.; Sargeson, A. M.; Smith, S. V. *Org. Biomol. Chem.* **2006**, *4*, 3350−3357.
(10) (a) Boswell, C. A.; Sun, X.; Niu, W.; Weisman, G. R.; Wong, E. H.; Rheingold, A. L.; Anderson, C. J. *J. Med. Chem.* **2004**, *47*, 1465−1474. (b) Woodin, K. S.; Heroux, K. J.; Boswell, C. A.; Wong, E. H.; Weisman, G. R.; Niu, W.; Tomellini, S. A.; Anderson, C. J.; Zakharov, L. N.; Rheingold, A. L. *Eur. J. Inorg. Chem.* **2005**, *23*, 4829−4833.
(11) Wong, E. H.; Weisman, G. R.; Hill, D. C.; Reed, D. P.; Rogers, M. E.; Condon, J. P.; Fagan, M. A.; Calabrese, J. C.; Lam, K. C.; Guzei, I. A.; Rheingold, A. L. *J. Am. Chem. Soc.* **2000**, *122*, 10561−10572.
(12) Ferdani, R.; Stigers, D. J.; Fiamengo, A. L.; Wei, L.; Li, B. T. Y.; Golen, J. A.; Rheingold, A. L.; Weisman, G. R.; Wong, E. H.; Anderson, C. J. *Dalton Trans.* **2012**, *41*, 1938−1950.
(13) Boros, E.; Cawthray, J. F.; Ferreira, C. L.; Patrick, B. O.; Adam, M. J.; Orvig, C. *Inorg. Chem.* **2012**, *51*, 6279−6284.
(14) Ferreiros-Martinez, R.; Esteban-Gomez, D.; Platas-Iglesias, C.; de Blas, A.; Rodriguez-Blas, T. *Dalton Trans.* **2008**, 5754−5765.
(15) Lima, L. M. P.; Esteban-Gomez, D.; Delgado, R.; Platas-Iglesias, C.; Tripier, R. *Inorg. Chem.* **2012**, *51*, 6916−6927.
(16) (a) Bevilaqua, A.; Gelb, R. I.; Hebard, W. B.; Zompa, L. J. *Inorg. Chem.* **1987**, *26*, 2699−2706. (b) Wieghardt, K.; Bossek, U.; Chaudhuri, P.; Herrmann, W.; Menke, B. C.; Weiss, J. *Inorg. Chem.* **1982**, *21*, 4308−4314.
(17) Šimeček, J.; Schulz, M.; Notni, J.; Plutnar, J.; Kubíček, V.; Havlíčková, J.; Hermann, P. *Inorg. Chem.* **2012**, *51*, 577−590.
(18) Šimeček, J.; Zemek, O.; Herrmann, P.; Wester, H. J.; Notni, J. *ChemMedChem* **2012**, *7*, 1375−1378.
(19) Ait-Mohand, S.; Fournier, P.; Dumulon-Perreault, V.; Kiefer, G. E.; Jurek, P.; Ferreira, C. L.; Bénard, F.; Guérin, B. *Bioconjugate Chem.* **2011**, *22*, 1729−1735.
(20) Šimeček, J.; Wester, H. J.; Notni, J. *Dalton Trans.* **2012**, *41*, 13803−13806.
(21) Fani, M.; Del Pozzo, L.; Abiraj, K.; Mansi, R.; Tamma, M. L.; Cescato, R.; Waser, B.; Weber, W. A.; Reubi, J.-C.; Maecke, H. R. *J. Nucl. Med.* **2011**, *52*, 1110−1118.
(22) Gasser, G.; Tjioe, L.; Graham, B.; Belousoff, M. J.; Juran, S.; Walther, M.; Künstler, J. U.; Bergmann, R.; Stephan, H.; Spiccia, L. *Bioconjugate Chem.* **2008**, *19*, 719−730.
(23) Palinkas, Z.; Roca-Sabio, A.; Mato-Iglesias, M.; Esteban-Gomez, D.; Platas-Iglesias, C.; de Blas, A.; Rodriguez-Blas, T.; Toth, E. *Inorg. Chem.* **2009**, *48*, 8878−8889.
(24) Stavila, V.; Allali, M.; Canaple, L.; Storzt, Y.; Franc, C.; Maurin, P.; Beuf, O.; Dufay, O.; Samarut, J.; Janier, M.; Hasserodt, J. *New J. Chem.* **2008**, *32*, 428−435.
(25) Mato-Iglesias, M.; Roca-Sabio, A.; Pálinkás, Z.; Esteban-Gómez, D.; Platas-Iglesias, C.; Tóth, É.; de Blas, A.; Rodríguez-Blas, T. *Inorg. Chem.* **2008**, *47*, 7840−7851.
(26) Wieghardt, K.; Bossek, U.; Chaudhuri, P.; Herrmann, W.; Menke, B. C.; Weiss, J. *Inorg. Chem.* **1982**, *21*, 4308−4315.
(27) Han, W.; Wang, Z.-D.; Xie, C.-Z.; Liu, Z.-Q.; Yan, S.-P.; Liao, D.-Z.; Jiang, Z.-H.; Cheng, P. *J. Chem. Crystallogr.* **2004**, *34*, 495−500.
(28) Corey, E. J.; Bailar, J. C., Jr. *J. Am. Chem. Soc.* **1959**, *81*, 2620−2629.
(29) Beattie, J. K. *Acc. Chem. Res.* **1971**, *4*, 253−259.
(30) Li, Q.-X.; Li, Q.; Chen, R.; Yang, X.-L.; Zhou, J.-Y.; Xu, H.-B. *Inorg. Chem. Commun.* **2010**, *13*, 1293−1295.
(31) Mameli, M.; Aragoni, M. C.; Arca, M.; Atzori, M.; Bencini, A.; Bazzicapuli, C.; Blake, A. J.; Caltaginore, C.; Devillanova, F. A.; Garau, A.; Hursthouse, M. B.; Isaia, F.; Lippolis, V.; Valtancoli, B. *Inorg. Chem.* **2009**, *48*, 9236−9249.
(32) Yang, R.; Zompa, L. J. *Inorg. Chem.* **1976**, *15*, 1499−1502.
(33) Van der Merve, M. J.; Boeyens, J. C. A.; Hancock, R. D. *Inorg. Chem.* **1985**, *24*, 1208−1213.
(34) Delgado, R.; Figueira, M. C.; Quintino, S. *Talanta* **1997**, *45*, 451−462.
(35) Chaudhuri, P.; Wieghardt, K. *Prog. Inorg. Chem.* **1987**, *35*, 329−436.
(36) Simulations of EPR spectra were performed with the SpinCount software, created by Prof. M. P. Hendrich at Carnegie Mellon University. SpinCount is available at http://www.chem.cmu.edu/groups/.
(37) (a) Hathaway, B. J.; Tomlinson, A. A. G. *Coord. Chem. Rev.* **1970**, *5*, 1−43. (b) Hathaway, B. J.; Billing, D. E. *Coord. Chem. Rev.* **1970**, *5*, 143−207. (c) Lever, A. B. P. *Inorganic Electronic Spectroscopy*, 2nd ed.; Elsevier: Amsterdam, 1984; pp 554−572. (d) Hathaway, B. J. *Coord. Chem. Rev.* **1983**, *52*, 87−169. (e) Lommens, P.; Feys, J.; Vrielinck, H.; De Buysser, K.; Herman, G.; Callens, F.; Van Driessche, I. *Dalton Trans.* **2012**, *41*, 3574−3582. (f) Rakhit, G.; Sarkar, B. *J. Inorg. Biochem.* **1981**, *15*, 233−241.
(38) Boswell, C. A.; Regino, C. A. S.; Baidoo, K. E.; Wong, K. J.; Milenic, D. E.; Kelley, J. A.; Lai, C. C.; Brechbiel, M. W. *Bioorg. Med. Chem.* **2009**, *17*, 548−552.
(39) Gervais, B.; Beuve, M.; Olivera, G. H.; Galassi, M. E. *Radiat. Phys. Chem.* **2006**, *75*, 493−513.
(40) Sun, X.; Wuest, M.; Weisman, G. R.; Wong, E. H.; Reed, D. P.; Boswell, C. A.; Motekaitis, R.; Martell, A. E.; Welch, M. J.; Anderson, C. J. *J. Med. Chem.* **2002**, *45*, 469−477.
(41) (a) *CrysAlis CCD, Version 1.171.33.52 (release 06−11−2009 CrysAlis171 .NET)*; Oxford Diffraction Ltd. (b) *CrysAlis RED, Version 1.171.33.52 (release 06−11−2009 CrysAlis171.NET)*; Oxford Diffraction Ltd.
(42) SHELX: Sheldrick, G. M. *Acta Crystallogr.* **2008**, *A64*, 112−122.
(43) Farrugia, L. J. *J. Appl. Crystallogr.* **1999**, *32*, 837−838.
(44) SIR97: Altomare, A.; Burla, M. C.; Camalli, M.; Cascarano, G. L.; Giacovazzo, C.; Guagliardi, A.; Moliterni, A. G. G.; Polidori, G.; Spagna, R. *J. Appl. Crystallogr.* **1999**, *32*, 115−119.

(45) Frisch, M. J.; Trucks, G. W.; Schlegel, H. B.; Scuseria, G. E.; Robb, M. A.; Cheeseman, J. R.; Scalmani, G.; Barone, V.; Mennucci, B.; Petersson, G. A.; Nakatsuji, H.; Caricato, M.; Li, X.; Hratchian, H. P.; Izmaylov, A. F.; Bloino, J.; Zheng, G.; Sonnenberg, J. L.; Hada, M.; Ehara, M.; Toyota, K.; Fukuda, R.; Hasegawa, J.; Ishida, M.; Nakajima, T.; Honda, Y.; Kitao, O.; Nakai, H.; Vreven, T.; Montgomery, J. A., Jr.; Peralta, J. E.; Ogliaro, F.; Bearpark, M.; Heyd, J. J.; Brothers, E.; Kudin, K. N.; Staroverov, V. N.; Kobayashi, R.; Normand, J.; Raghavachari, K.; Rendell, A.; Burant, J. C.; Iyengar, S. S.; Tomasi, J.; Cossi, M.; Rega, N.; Millam, N. J.; Klene, M.; Knox, J. E.; Cross, J. B.; Bakken, V.; Adamo, C.; Jaramillo, J.; Gomperts, R.; Stratmann, R. E.; Yazyev, O.; Austin, A. J.; Cammi, R.; Pomelli, C.; Ochterski, J. W.; Martin, R. L.; Morokuma, K.; Zakrzewski, V. G.; Voth, G. A.; Salvador, P.; Dannenberg, J. J.; Dapprich, S.; Daniels, A. D.; Farkas, Ö.; Foresman, J. B.; Ortiz, J. V.; Cioslowski, J.; Fox, D. J. *Gaussian 09, Revision A.01*; Gaussian, Inc.: Wallingford, CT, 2009.
(46) Tao, J. M.; Perdew, J. P.; Staroverov, V. N.; Scuseria, G. E. *Phys. Rev. Lett.* **2003**, *91*, 146401.
(47) Schaefer, A.; Horn, H.; Ahlrichs, R. *J. Chem. Phys.* **1992**, *97*, 2571−2577.
(48) Stanton, J. F.; Gauss, J. *Adv. Chem. Phys.* **2003**, *125*, 101−146.
(49) Montoya, A.; Truong, T. N.; Sarofim, A. F. *J. Phys. Chem. A* **2000**, *124*, 6108−6110.
(50) Tomasi, J.; Mennucci, B.; Cammi, R. *Chem. Rev.* **2005**, *105*, 2999−3093.
(51) Hedegard, E. D.; Kongsted, J.; Sauer, S. P. A. *J. Chem. Theory Comput.* **2011**, *7*, 4077−4087.
(52) Rega, N.; Cossi, M.; Barone, V. J. *J. Chem. Phys.* **1996**, *105*, 11060−11067.
(53) Zbiri, M. *Inorg. Chim. Acta* **2006**, *359*, 3865−3870.
(54) Rossotti, F. J.; Rossotti, H. J. *J. Chem. Educ.* **1965**, *42*, 375−378.
(55) Schwarzenbach, G.; Flaschka, W. *Complexometric Titrations*; Methuen & Co.: London, 1969.
(56) Gans, P.; Sabatini, A.; Vacca, A. *Talanta* **1996**, *43*, 1739−1753.
(57) Alderighi, L.; Gans, P.; Ienco, A.; Peters, D.; Sabatini, A.; Vacca, A. *Coord. Chem. Rev.* **1999**, *184*, 311−318.